






Center drill geometry mapping in friction drilling of aluminium 6063 using artificial neural network approach

Yogesh Ganpat Kamble^{1*}, Rajiv B.², Vipul Prabhakar Rathod¹,
Prakash Pantawane², Sandeep Wankhade³

¹ Department of Robotics and Automation Engineering, D Y Patil College of Engineering,
Akurdi Pune Maharashtra 411044, India

² Department of Manufacturing Science and Engineering, COEP Tech University Pune Maharashtra,
411005, India

³ Department of Mechanical Engineering, AISSMS COE, Pune, Maharashtra 411 001, India

* Corresponding author's email: yogeshkamble2912@gmail.com

ABSTRACT

The growing demand for rapid production and innovative joining methods in the automotive, tube manufacturing, mechanical, and civil engineering sectors has led to the development and application of advanced hole-making techniques. One such technique is the friction drilling process, also referred to as thermal drilling, form drilling, or flow drilling, which utilizes the frictional heat generated between a rotating conical tool and the workpiece to produce holes without traditional cutting. This nontraditional process displaces material using a combination of axial force and rotational speed, allowing the tool to penetrate and plastically deform the substrate to form a bush or collar-like structure surrounding the hole without producing chips. The technique is highly effective on ductile and thermally conductive materials like aluminum 6063, offering increased structural integrity and material efficiency. The bush formed is typically 1.5 to 2.5 times thicker than the original tube wall, enhancing joint strength for tubular and sheet metal applications. This paper presents an experimentation of the friction drilling process on Aluminium tubes of varying thickness using High Speed Steel Center Drill (ASTM 600), drill tool of different tip angle.

Keywords: centre drill, plain center drill, slotted center drill, circularity error, roundness error.

INTRODUCTION

Friction drilling is an innovative, chip less machining process that uses heat generated from friction to pierce holes in metal without producing any metal chips. Unlike traditional drilling methods, this process relies on a rotating conical tool that softens the material through intense frictional heat and then pushes through it to form a clean hole with an extended collar or bush. The process begins when the tip of the center drill contacts the workpiece surface. As the tool rotates and moves forward, the material heats up, becomes soft, and is plastically deformed. The conical part of the tool forms the initial hole, while the cylindrical part helps shape the collar. Eventually, the shoulder of the tool forms a ring or boss on the surface,

creating a durable, dimensional hole. The bush formed through this process is typically 1.5 to 2.5 times thicker than the original material, providing strong joints and structural integrity.

Friction drilling works effectively on a variety of metals, especially non-ferrous materials like aluminum 6063 and 6082, making it ideal for applications in industries requiring lightweight and strong assemblies. The process has several advantages: it ensures good dimensional accuracy, creates strong and clean joints capable of bearing high loads, and requires no lubricants. It also eliminates chip formation, reducing material waste and making it suitable for automation. The method is highly adaptable, capable of forming holes even in blind or hard-to-reach sections.

In practical applications, friction drilling finds extensive use in the automobile industry, for joining multiple frames, seat frames, foot pedals, fuel rails, and exhaust parts. It is also widely used in hospital equipment, agriculture (such as seed delivery systems), and the pharmaceutical sector for securely fastening tubes and pipes. Its ability to form strong, reliable, and clean holes makes it a valuable process in modern manufacturing systems where efficiency and joint quality are critical [1, 2].

Several studies have examined the wear characteristics of tools used in the friction drilling process. Various investigation on tool wear behavior using tungsten carbide tools on low carbon steel are experimented [3, 4] using SEM, spectroscopy, and thermal imaging to analyze how tool geometry and elevated temperatures (above 260 °C) influenced tool life and overall performance [5]. The carbide tools possess superior wear resistance and maintain structural integrity during prolonged use. PVD-coated conical tools with uncoated tools, finding that coatings significantly reduced wear and improved temperature tolerance, resulting in better hole quality [6]. However, they also observed that repeated drilling led to performance degradation.

The designed sintered carbide drills and modified them for optimal performance on austenitic stainless steel [7]. Experiments conducted using Taguchi design of experiments, evaluated that surface roughness and shape accuracy and reported enhanced outcomes compared to standard drills. studied the influence of tool geometry and material properties on thrust force and torque in the drilling of AA-6351 aluminum alloy. Moreover, mathematical modeling performed indicated that the conical angle and pipe thickness were key performance factors [8, 9]. Micro center drills for tool steel and used artificial neural networks (ANN) to predict thrust force based on varying spindle speed and feed rate. A hybrid drill-tap tool made of high-speed steel (HSS) and found that the conical region of the tool was the most wear-prone. Compared with conventional tools, their tool design showed better bush formation and process efficiency [10].

The effectiveness of friction drilling heavily depends on process parameters such as spindle speed, feed rate, and conical angle. identified spindle speed and feed as the most influential factors affecting hole quality [11]. The high-speed rotation was crucial for clean hole formation and demonstrated, through thermal analysis, that materials with better thermal conductivity and creep

resistance yielded superior surface finishes. analyzed bush height and material stress during drilling of mild steel and aluminum. Additionally, software-based simulations provided insights into deformation behavior under varying loads [12, 13].

Materials with low conductivity often failed to soften adequately, resulting in poor hole quality [14] this emphasized the importance of preheating in such cases and identified feed rate as the dominant factor affecting bush length. focused on Al 6063 and 6082, observing torque variations, ductility changes, and surface cracking [15]. The dynamometers to measure thrust and torque, asserting that the relationship among speed, feed, and material thickness is critical for dimensional accuracy, high heat zones as areas needing precise control to avoid deformation [16, 17].

Heat generation and distribution are central to understanding friction drilling dynamics. used 3-Deform software to simulate 3D thermal zones, material flow, and phase transformations. Analysis revealed critical areas around the tool tip and tool-work interface that experience intense thermal activity [18]. The thermal effects during post-drilling threading showed that the conical and collar regions of the workpiece are most affected by temperature. They compared thread forming and cutting, concluding that thread forming generates less heat and yields stronger threads [19, 20].

The properties of the workpiece material significantly impact the outcomes of friction drilling. performed comparative studies on mild steel and aluminum, demonstrating that ductility and thermal behavior affect bush formation and deformation [21, 22]. Similarly investigated that natural fiber-reinforced composites, specifically jute-based materials, and found that curing temperature and fiber content greatly influence hole quality and delamination levels [23, 24].

Comparing center drills and traditional drills on sheet metal, noting that traditional drills required less thrust due to their flute geometry [25] examined brittle pipes and observed petal-like cracks and surface fractures during drilling [26]. Using ABAQUS software, they modeled crack depth, displacement, and mesh behavior under stress. studied hybrid composites, utilizing spectroscopy and hardness testing to evaluate material changes post-drilling [27, 28].

Modern friction drilling research increasingly integrates optimization methods to enhance output parameters such as bush length, diameter, and thrust force. combined the Taguchi method with

fuzzy logic to optimize the drilling of stainless steel, focusing on maximizing bush length [29]. conducted multi-objective statistical optimization, correlating spindle speed, feed, and conical angle with bush formation characteristics [30, 31].

METHODOLOGY

Selection of tool

The center drilling tool, made from High Speed Steel Center Drill (ASTM 600) grade high-speed steel, is specifically selected for its excellent mechanical properties, cost-effectiveness, and versatility across various industrial sectors. High Speed Steel Center Drill (ASTM 600) steel finds wide application in the manufacturing industry, agricultural field, and even the aerospace sector, primarily due to its capacity to perform reliably under heavy load and at elevated temperatures. It exhibits significant wear resistance, which is crucial for extended tool life during demanding operations. In comparison to more expensive materials like tungsten carbide, High Speed Steel Center Drill (ASTM 600) offers a balanced combination of hardness, toughness, and economic feasibility. The typical alloy composition of High Speed Steel Center Drill (ASTM 600) steel includes approximately 0.86% carbon (C), 4% chromium (Cr), 5% molybdenum (Mo), 6% tungsten (W), and 2% vanadium (V). Each of these alloying elements plays a critical role in enhancing hardness, strength, and thermal stability of the material. To further improve the performance and durability of the center drill, a systematic heat treatment process is carried out. This heat treatment significantly increases the material's hardness from its original state to around 55 to 58 HRC, making it more suitable for high-stress machining operations. The goal of heat-treating high-speed steels like High Speed Steel Center Drill (ASTM 600) is to transform the soft, annealed microstructure which primarily consists of ferrite and carbides into a hardened and tempered martensitic structure. This martensitic transformation, along with the presence of fine carbides, imparts the necessary hardness and wear resistance to the cutting tool.

The heat treatment process is typically carried out in four major stages: preheating, austenitizing, quenching, and tempering. In the preheating stage, the tool is gradually heated to reduce

thermal shock. Sudden exposure of a cold tool to high furnace temperatures could cause it to crack, hence this stage helps in minimizing such risks. Following this is the austenitizing stage, which is a time and temperature-controlled process. Here, the tool is heated to a high enough temperature that allows complex alloy carbides to dissolve into the austenite phase, preparing the material for the hardening transformation.

The tool undergoes the quenching process, where it is rapidly cooled, first in a molten salt bath or oil, followed by air cooling. This rapid cooling transforms the austenitic structure into hard martensite, giving the tool its necessary hardness. However, martensite is inherently brittle, so to enhance the toughness and relieve internal stresses induced during quenching, the tool is subjected to the tempering process. During tempering, the material is reheated to a moderate temperature to reduce brittleness, convert retained austenite to martensite, and make the steel more robust and reliable in practical applications (Table 1) (Figures 1–3).

SELECTION OF WORKPIECE

For experimentation tubes of aluminium 6063 material of various thickness has been utilized. The selected material has aluminium as principle material that has various applications in field automotive, aerospace, biomedical, optics etc. Aluminium alloy 6063 is light weight material that shows high strength and weight ratio.

In addition, it has an elastic modulus like 70 GPa; as a result, about one-third of the elastic modulus of many types of steel and its allied materials. So, an enumeration of various experimental results, deformation of the work material is vital to the accuracy of the targeted hole (Table 2, 3).

Chemical composition of varying thickness of workpiece material AL 6063. Making center drill requires selection of material along with its chemical and mechanical composition after that heat treatment processing and finally finishing by diamond grinding. So, the same is applicable for workpiece material by knowing its properties so that it will be beneficial to implement several combinations of parameters over the friction drilling process.

To effectively examine and optimize these variables, both experimental and numerical approaches have been adopted. For planning the

Table 1. Center drill tool geometry with varying conical angle

Dia.	D	Mm	7.8	7.8	7.8
Tip angle	A	degree	90	90	90
Conical angle	β	degree	36	39	42
Center region	length hc	mm	0.979	0.983	0.997
Conical region	length hn	mm	7	7	7
Cylindrical region	length hl/dia	mm	17/7.8	17/7.8	17/7.8
Shoulder region	length/dia	mm	5/10	5/10	5/10
Shank region	length/dia	Mm	20/7.8	20/7.8	20/7.8

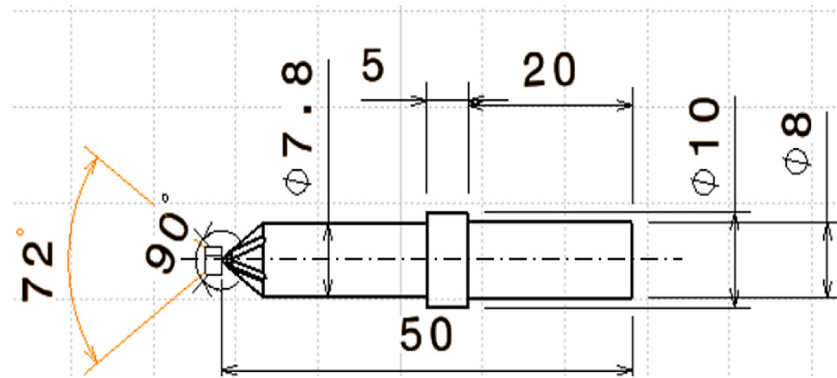


Figure 1. Slotted center drill with a conical angle of 36°

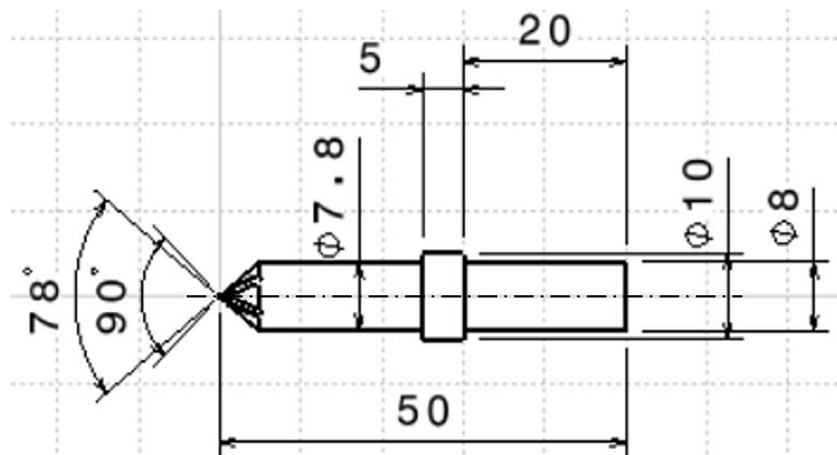


Figure 2. Slotted center drill with a conical angle of 39°

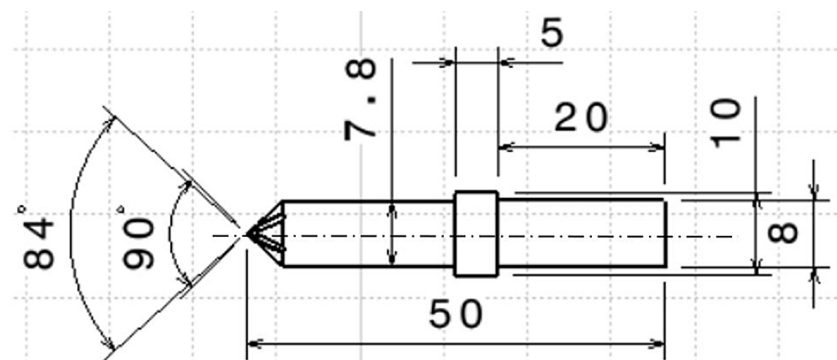


Figure 3. Slotted center drill with a conical angle of 42°

Table 2. Mechanical properties of Al 6063

Workpiece thickness (mm)	Ultimate tensile strength (N/m)	Yield strength (N/m)	Elongation (%)	Yield load (kN)	Ultimate load (kN)	Hardness (HV) at 5 kG load	Melting temperature (°C)	Density (kg/m ³)	Thermal conductivity
1.5	232.66	190.22	24.97	6.5	7.95	79.7	600	2700	200
2.25	162.68	139.76	16.56	7.35	8.55	62.6			
3	159.3	126.72	15.81	7	8.8	52.6			

Table 3. Chemical composition of workpiece

Name of the element	Al	Mn	Si	Cu	Zn	Ti	Fe	Mg
Weight percentage	98.63	0.034	0.349	0.084	0.085	0.034	0.134	0.594

experiments, the, the well-known Box-Behnken design (BBD) is employed, which is a part of the response surface methodology (RSM) framework. This method allows for efficient experimentation while minimizing the number of required trials. Box-Behnken design with 4 continuous and one categorical factor has been selected.

One of the key advantages of BBD is that it avoids extreme combinations of parameters such as setting all variables to their maximum or minimum simultaneously. This not only reduces the risk of damaging equipment or producing unreliable results but also ensures a balanced and safe experimental plan. A plain center drill (PCD) is a solid tool without any slot or flute along its body. It is typically used in friction drilling or center drilling processes where the tool heats and displaces the material to form a hole or starting point for further machining. A slotted center drill (SCD) features axial or helical slots along its body (Figure 4).

ANOVA BBD is employed with spindle speed ranging from 2500–5500 rpm which is optimum for frictional drilling of soft material like aluminium. For feed rate, a range of 50 to 80 mm/min was selected based on the machine tool's capabilities, which allow up to 100 mm/min without slippage or excessive wear. Preliminary trials indicated that feeds below 50 mm/min lead to excessive localized heat generation, adversely affecting hole quality and tool life. Therefore, a uniform step size of 15 mm/min was chosen to ensure both process stability and comparative analysis. Experiments were conducted on Aluminium Tubes of varying thickness, using High Speed Steel Center Drill with different conical angle using plain and slotted center drill (Table 4 and Figure 5).

RESULTS AND DISCUSSION

ANOVA table consist of sources that explains different factors or sources of variation in experiment, contribution Shows which factor is more influential in affecting the result.

Adjusted sum of squares is amount of variation attributed to each source after adjusting for other factors in the model and Adjusted Mean Square average variation for each source. F-value compares the variation between group means (due to the factor) to the variation within the groups (error), Higher F-value suggests more likely the factor is statistically significant. P-value is the probability that the observed differences are due to random chance, $P < 0.05$, the factor is considered statistically significant.

Thrust force

The ANOVA Table 5 presents the statistical analysis of five input parameters on thrust force. Among these, Speed shows the most significant influence, contributing approximately 27.16% to the overall variation with a P-value of 0.000, indicating a highly significant effect. Thickness also plays a strong role, contributing 15.66%, and is statistically significant with a P-value of 0.000. Feed, tip angle and tool type contribute about 4 % with moderately significant P-value is 0.046, 0.049 and 0.05 meaning it has a noticeable, though smaller, impact. The overall model's R-squared value is 68.36% that suggests the model is fairly reliable.

It is found that with increase in spindle speed thrust force seems to decrease. While with increase in tip angle area thrust force shows slight increase. For higher speed and lower tip angle

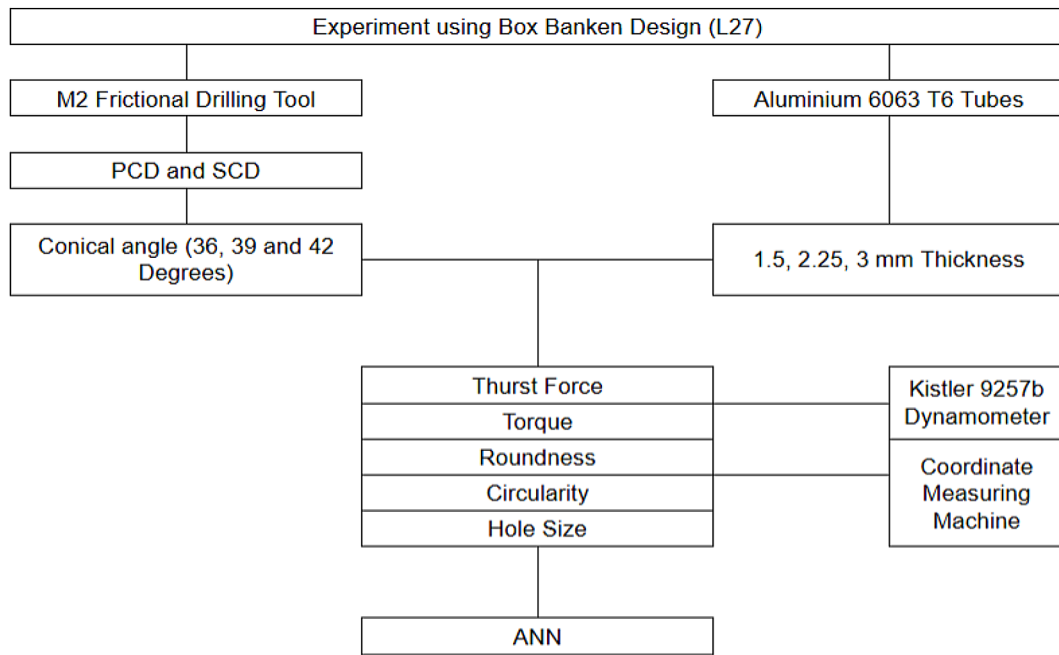


Figure 4. Methodology

Table 4. Design of experiment

Levels and parameters	Spindle speed (RPM)	Feed (mm/min)	Workpiece thickness (mm)	Conical angle (degrees)	Type of tool
-1	2500	50	1.5	36	PCD and SCD
0	4000	65	2.25	39	
1	5500	80	3	42	

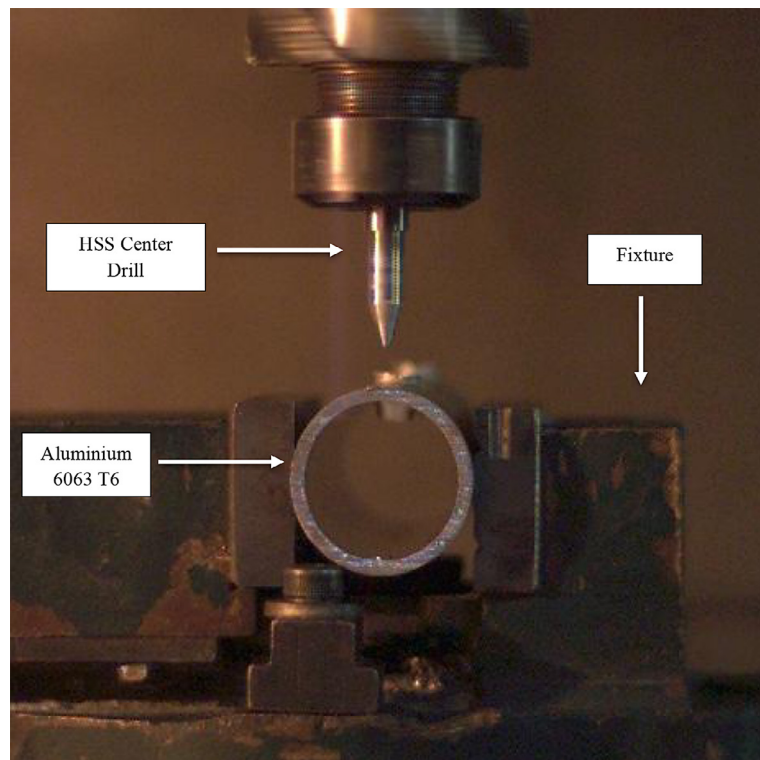


Figure 5. Experimental setup

Table 5. ANOVA for thrust force

Source	Contribution	Adj SS	Adj MS	F-value	P-value
Tip angle	0.89%	2269	2269.3	4.07	0.051
Speed	29.76%	75734	75734.5	27.16	0
Feed	3.98%	10135	10134.6	4.17	0.046
Thickness	18.78%	47788	47788	15.66	0
Tool type	0.76%	1927	1926.8	4.03	0.05
Error	45.83%	116649	2430.2		
Total	100.00%				
R-sq	83.36%				

less thrust force is observed, which can be confirmed in surface plot that higher spindle speed and lower tip angle is favorable as it produces lower thrust force as a result less load is applied on tool and machine.

It is found that with increase in spindle speed thrust force seems to decrease. While with increase in feed thrust force shows slight increase. For higher speed and lower feed less thrust force is observed, which can be confirmed in surface plot that higher spindle speed and lower feed is favorable as it produces lower thrust force as a result less load is applied on tool and machine.

It is found that with increase in spindle speed thrust force seems to decrease whereas with increase in thickness of thrust force increase. For

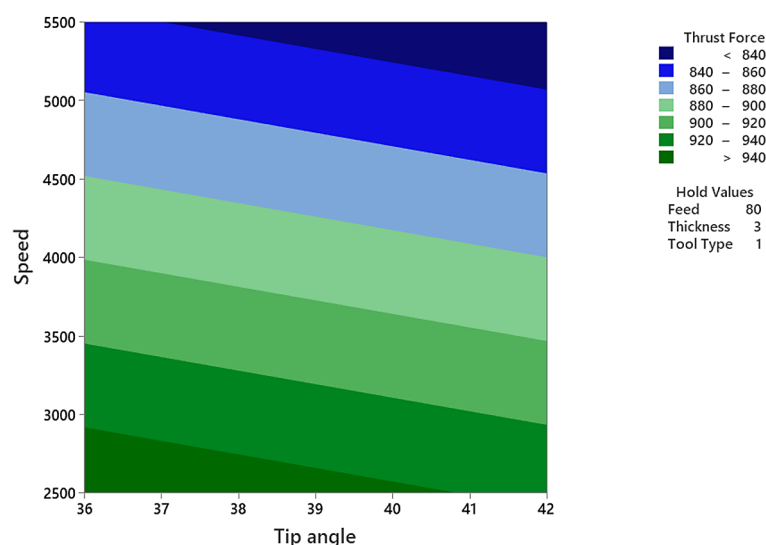
higher speed and less thickness less thrust force is observed, which can be confirmed in surface plot that higher spindle speed and lower thickness is favorable as it produces lower thrust force as a result less load is applied on tool and machine (Table 6 and Figures 6–11).

Torque

The ANOVA Table 7 for torque shows that Speed is the most significant factor, contributing 49.81% to the overall variation with a P-value of 0.000, making it highly significant. Feed and Thickness also have a noticeable impact, contributing 5.67% and 4.71% respectively, with P-values of 0.015 and 0.026, indicating

Table 6. Trend of main effect plot for thrust force

Output variable	Tip angle	Speed	Feed	Thickness	Tool type
Thrust force	Negative	Negative	Negative	Positive	Negative


Figure 6. Contour plot of thrust force vs speed, tip angle

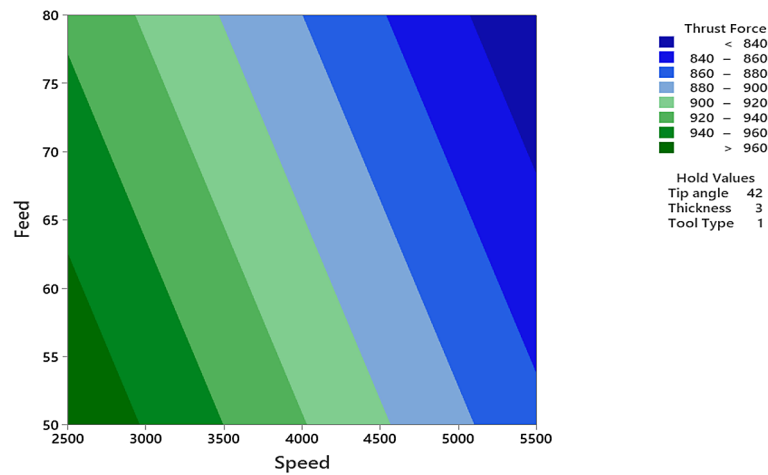


Figure 7. Contour plot of thrust force vs feed, speed

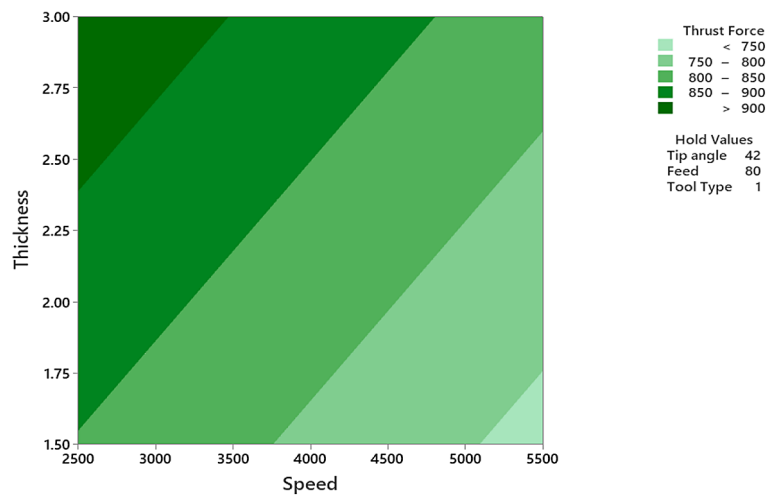


Figure 8. Contour plot of thrust force vs thickness, speed

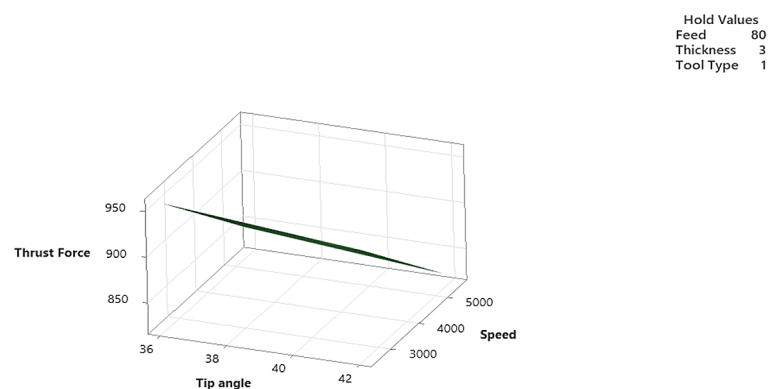


Figure 9. Surface plot of thrust force vs speed, tip angle

statistical significance. On the other hand, tip angle and tool type contribute very little, with p value of 0.049 and 0.05. The model has an R-squared value of 85.41%, which suggests that the selected factors explain a good portion of

the variation in torque, making the model reliable for prediction.

It is found that with increase in spindle speed torque seems to decrease. While with increase in tip angle area torque shows slight increase. For

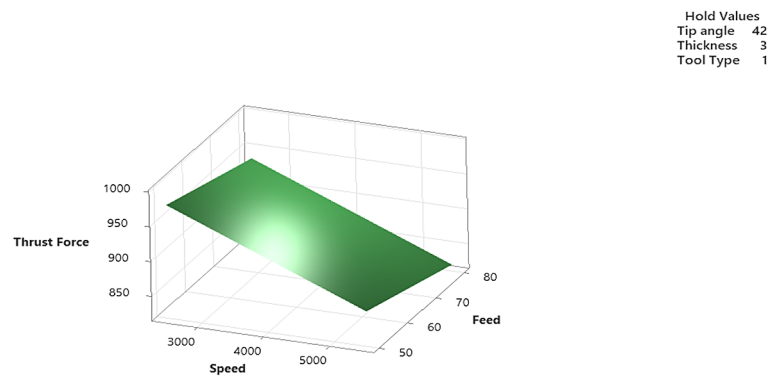


Figure 10. Surface plot of thrust force vs feed, speed

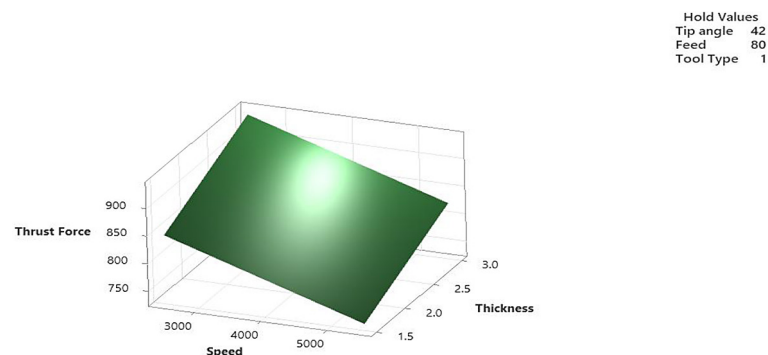


Figure 11. Surface plot of thrust force vs speed, tip angle

Table 7. ANOVA for Torque

Source	Contribution	Adj SS	Adj MS	F-value	P-value
Tip angle	0.01%	0.0123	0.0123	1.21	0.049
Speed	46.84%	39.8559	39.8559	49.81	0
Feed	5.67%	4.8223	4.8223	6.39	0.015
Thickness	4.71%	4.0107	4.0107	5.31	0.026
Tool type	0.18%	0.1533	0.1533	1.2	0.05
Error	42.58%	36.2284	0.7548		
Lack-of-fit	42.45%	36.1174	0.8209	29.59	0.002
Pure error	0.13%	0.111	0.0277		
Total	100.00%				
R - Sq	85.41%				

higher speed and lower tip angle less torque is observed, which can be confirmed in surface plot that higher spindle speed and lower tip angle is favorable as it produces lower torque as a result less load is applied on tool and machine.

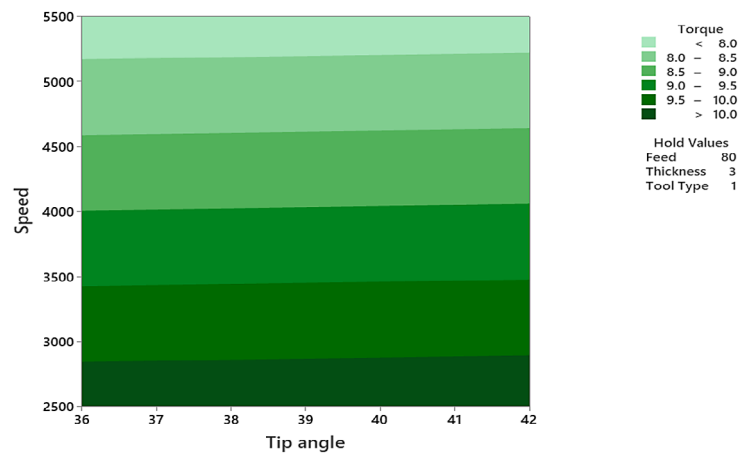
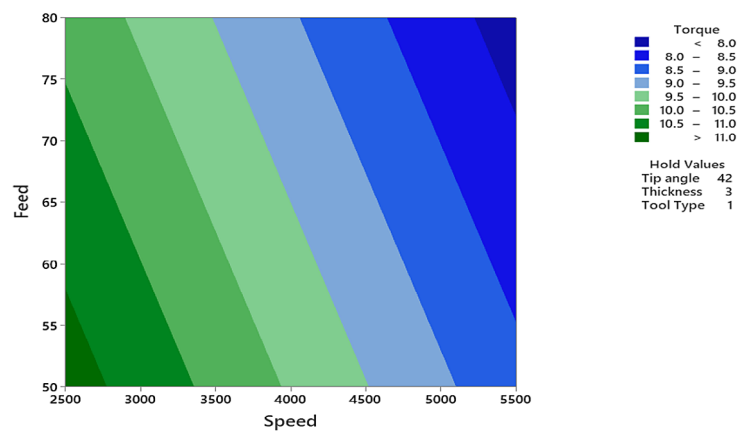
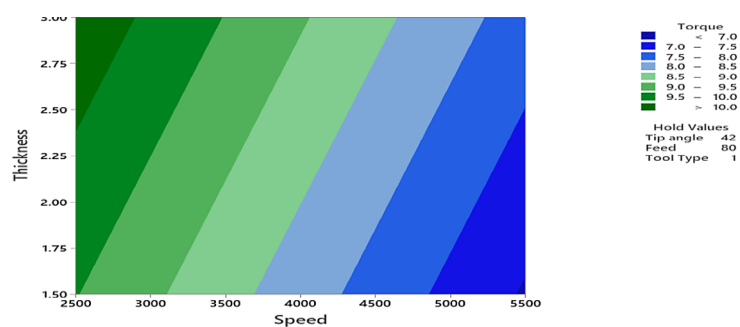
It is found that with increase in spindle speed torque seems to decrease. While with increase in feed torque shows slight increase. For higher speed and lower feed less torque is observed, which can be confirmed in surface plot that higher spindle speed and lower feed is favorable as it

produces lower torque as a result less load is applied on tool and machine.

It is found that with increase in spindle speed torque seems to decrease whereas with increase in thickness of thrust force increase. For higher speed and less thickness less torque is observed, which can be confirmed in surface plot that higher spindle speed and lower thickness is favorable as it produces lower torque as a result less load is applied on tool and machine (Table 8 and Figures 12–17).

Table 8. Trend of main effect plot for torque

Output variable	Tip angle	Speed	Feed	Thickness	Tool type
Torque	Negative	Negative	Negative	Positive	Positive


Figure 12. Contour plot of torque vs speed, tip angle

Figure 13. Contour plot of torque vs feed, speed

Figure 14. Contour plot of torque vs thickness, speed

Roundness error

In the case of roundness error, Speed again shows a major influence, contributing 54.31% with a P-value of 0.000, confirming its high

significance. Feed also plays a moderate role, accounting for 5.18% of the variation with a P-value of 0.027. Tip angle, thickness and tool type contributes around 4.19% and is borderline

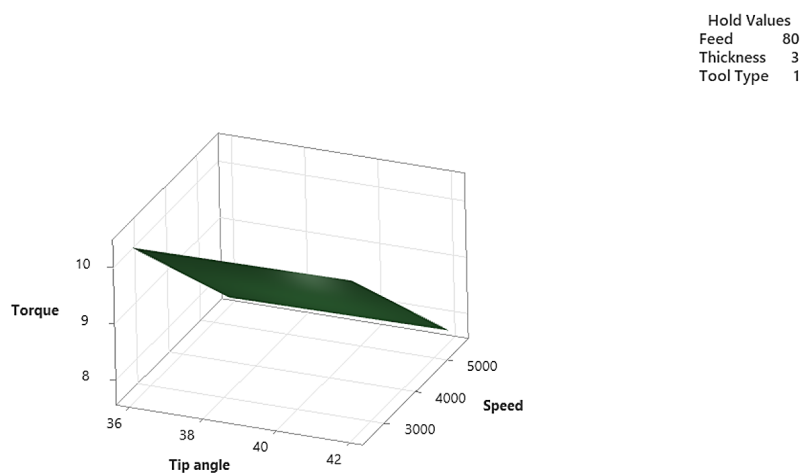


Figure 15. Surface plot of torque vs speed, tip angle

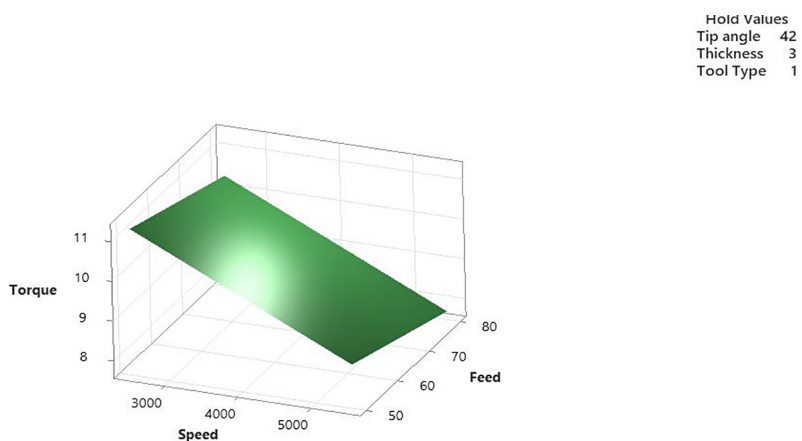


Figure 16. Surface plot of torque vs feed, speed

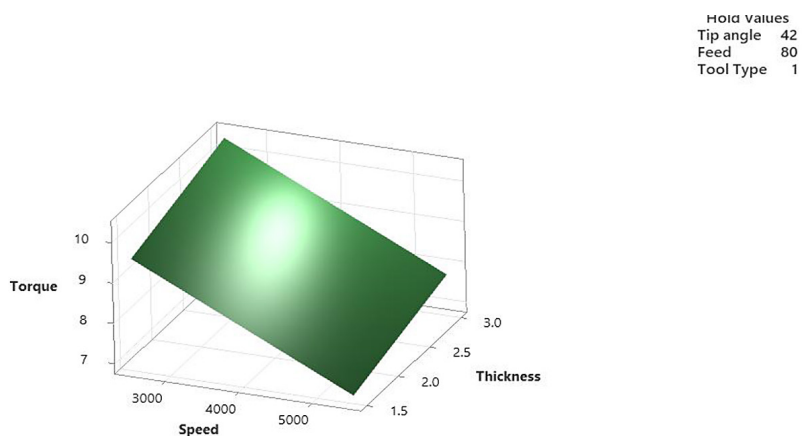


Figure 17. Surface plot of torque vs speed, tip angle

significant with a P-value. However, with an R-squared value of 81.41%, this model provides a good explanation of the variation in roundness error, reflecting a solid fit (Table 9).

The increase in spindle speed leads to improved roundness error, meaning the holes become more uniform. A higher tip angle causes a slight increase in roundness error, making the hole

Table 9. ANOVA for roundness error

Source	Contribution	Adj SS	Adj MS	F-Value	P-Value
Tip angle	4.19%	0.000485	0.000485	4.89	0.032
Speed	48.19%	0.005577	0.005577	54.31	0
Feed	4.44%	0.000513	0.000513	5.18	0.027
Thickness	1.70%	0.000196	0.000196	2.98	0.046
Tool type	0.42%	0.000049	0.000049	1.49	0.051
Error	41.07%	0.004753	0.000099		
Total	100.00%				
R - Sq	81.41%				

shape slightly less accurate. For higher speed and lower tip angle less roundness error is observed, which can be confirmed in surface plot that higher spindle speed and lower tip angle is favorable as it produces lower roundness error.

It is found that with increase in spindle speed roundness error seems to decrease. While with increase in feed roundness error shows slight increase. For higher speed and lower feed less roundness error is observed, which can be confirmed in surface plot that higher spindle speed and lower feed is favorable as it produces lower roundness error.

It is found that with increase in spindle speed roundness error seems to decrease whereas with increase in thickness of roundness error increase. For higher speed and less thickness less roundness error is observed, which can be confirmed in the surface plot that higher spindle speed and

lower thickness is favorable as it produces lower roundness error (Table 10 and 18–23).

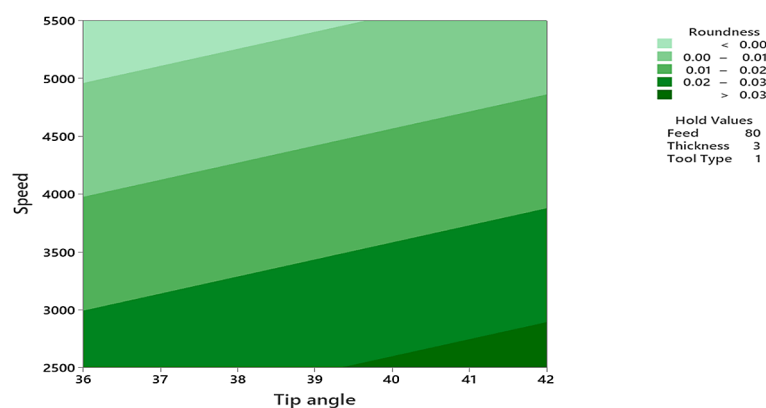
Cylindricity errors

For cylindricity errors, the tool type stands out as the only significant factor, contributing 49.44% with a P-value of 0.029. All other parameters show very low contributions tip angle and spindle speed has P-value of 0.02 that suggests it has good impact whereas feed and thickness of tool contributes less of about 3% and are slightly significant. The overall R-squared value is 83.33%, indicating the model explains a moderate portion of the variability in cylindricity errors, but still leaves room for improvement (Table 11).

The increase in spindle speed leads to improved cylindricity errors, meaning the holes become more uniform. A higher tip angle causes a slight increase in cylindricity errors, making the

Table 10. Trend of main effect plot for roundness error

Output variable	Tip angle	Speed	Feed	Thickness	Tool type
Roundness error	Positive	Negative	Negative	Negative	Negative

**Figure 18.** Contour plot of roundness error vs speed, tip angle

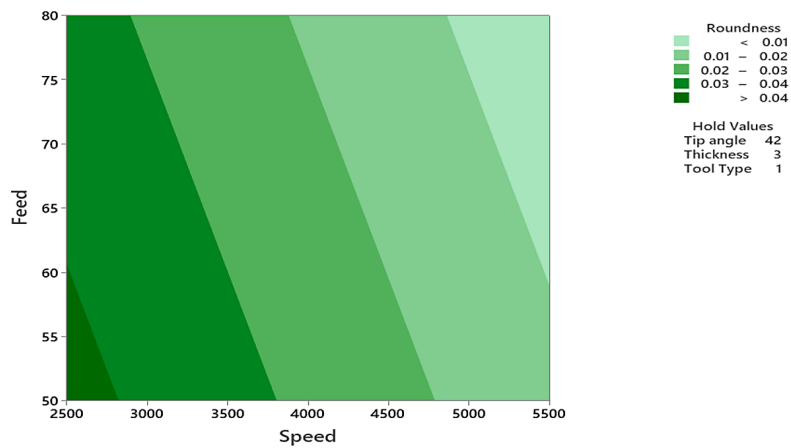


Figure 19. Contour plot of roundness error vs feed, speed

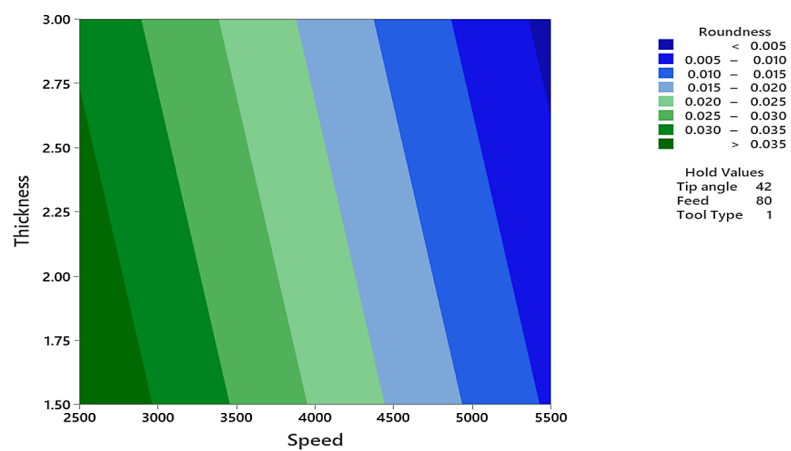


Figure 20. Contour plot of roundness error vs thickness, speed

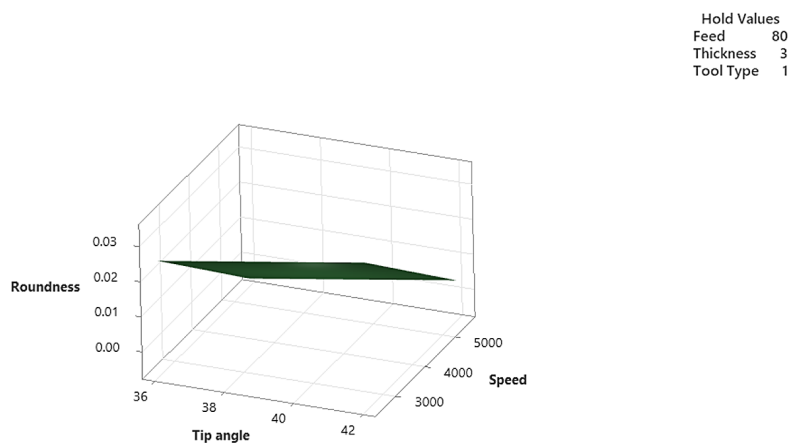


Figure 21. Surface plot of roundness error vs speed, tip angle

hole shape slightly less accurate. For higher speed and lower tip angle less cylindricity errors is observed, which can be confirmed in surface plot that higher spindle speed and lower tip angle is favorable as it produces lower cylindricity errors.

The higher spindle speeds consistently lead to improved cylindricity errors. While with increase in feed roundness error shows slight increase in cylindricity errors error. For higher speed and lower feed less cylindricity errors is observed,

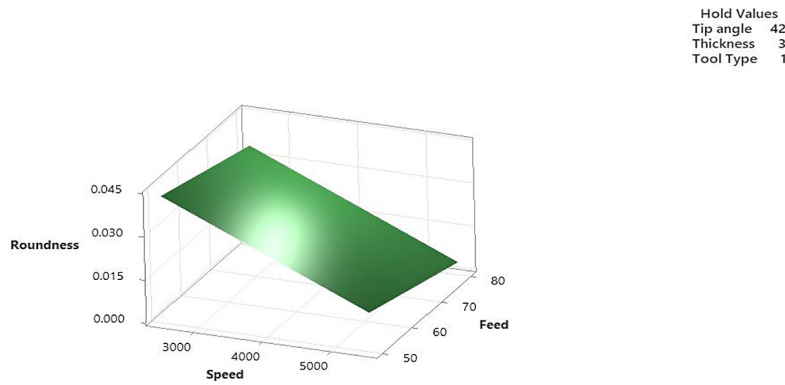


Figure 22. Surface plot of roundness error vs feed, speed

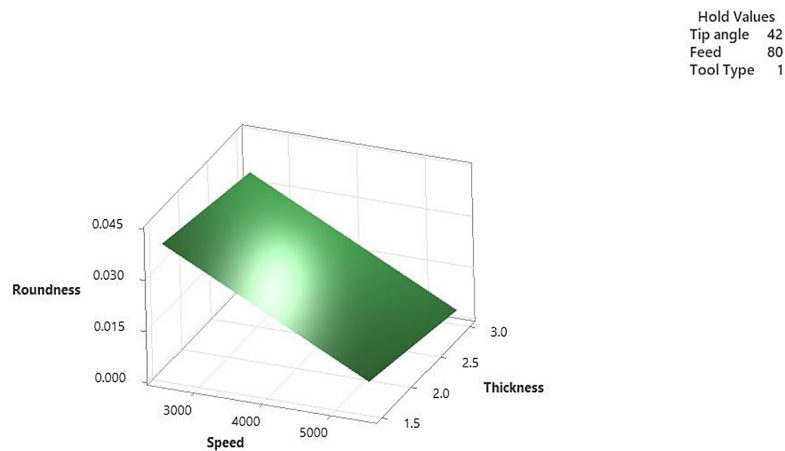


Figure 23. Surface plot of roundness error vs speed, tip angle

Table 11. ANOVA for cylindricity errors

Source	Contribution	Adj SS	Adj MS	F-Value	P-Value
Tip angle	7.21%	0.000031	0.000031	4.89	0.023
Speed	8.83%	0.00155	0.00155	5.89	0.02
Feed	4.48%	0.000069	0.000069	2.98	0.041
Thickness	4.64%	0.000089	0.000089	2.49	0.05
Tool type	49.44%	0.007082	0.007082	53.41	0.00
Error	25.40%	0.067251	0.001401		
Total	100.00%				
R - Sq	83.33%				

Table 12. Trend of main effect plot for cylindricity errors

Output variable	Tip angle	Speed	Feed	Thickness	Tool type
Cylindricity errors	Negative	Negative	Positive	Negative	Positive

which can be confirmed in surface plot that higher spindle speed and lower feed is favorable as it produces lower cylindricity error (Table 12).

It is found that with increase in spindle speed cylindricity errors seems to decrease

whereas with increase in thickness of cylindricity errors increase. For higher speed and less thickness less cylindricity errors is observed, which can be confirmed in surface plot that higher spindle speed and lower thickness is

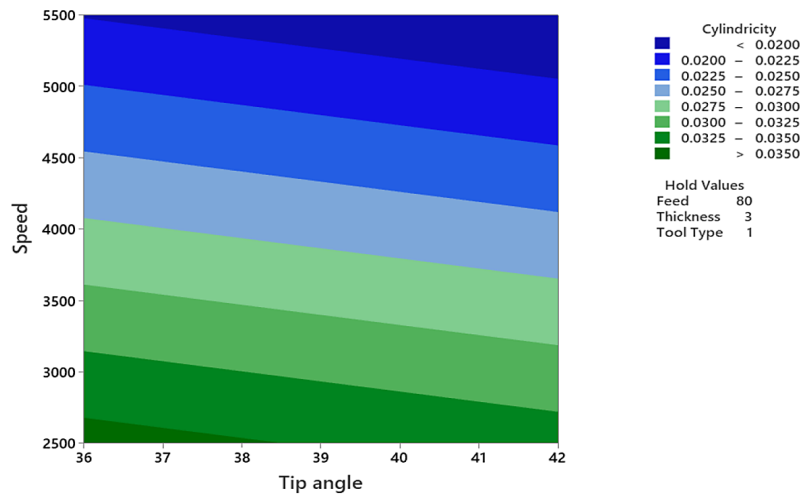


Figure 24. Contour plot of cylindricity errors vs speed, tip angle

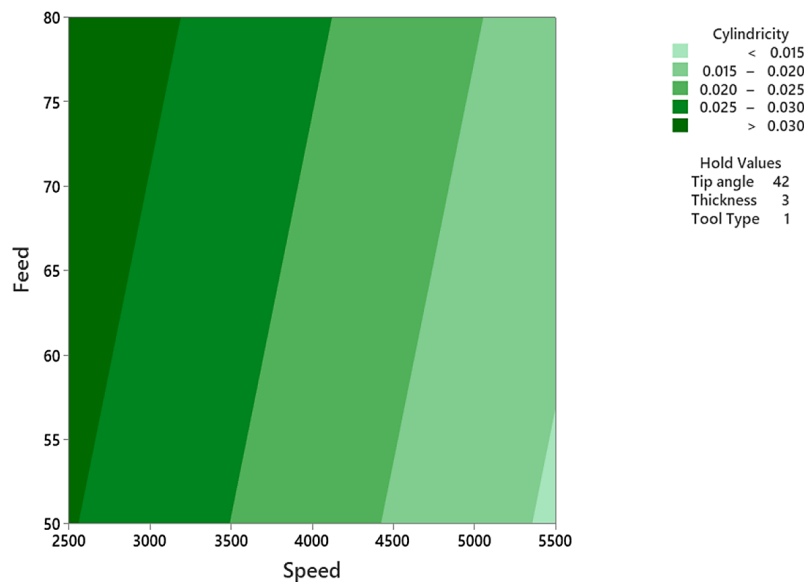


Figure 25. Contour plot of cylindricity errors vs feed, speed

favorable as it produces lower cylindricity errors (Figures 24–29).

Hole size

In the analysis of Hole size, the most influential factor is tool type, which alone contributes 45.93% of the variation and is highly significant with a P-value of 0.000. Feed and speed contributes about 14% and are statistically significant, whereas Tip angle and thickness contributes little. Tip angle is moderately significant and thickness of workpiece is not significant. The R-squared value of 87.32% suggests that the model captures a reasonable amount of the variation in hole size (Table 13).

The increase in spindle speed leads to the hole size tends to increase slightly, indicating thermal expansion or reduced cutting resistance at high speed. A higher tip angle tends to slightly reduce the hole size, potentially due to increased axial pressure and altered chip evacuation. For higher speed and lower tip angle slightly larger and more consistent hole sizes is observed, which can be confirmed in surface plot that higher spindle speed and lower tip angle is favorable as it produces better hole size.

The higher spindle speed again slightly increases the hole size. While with increase in feed small reduction in hole size is observed. For higher speed and lower feed less produce hole size nearer to expected, which can be confirmed in

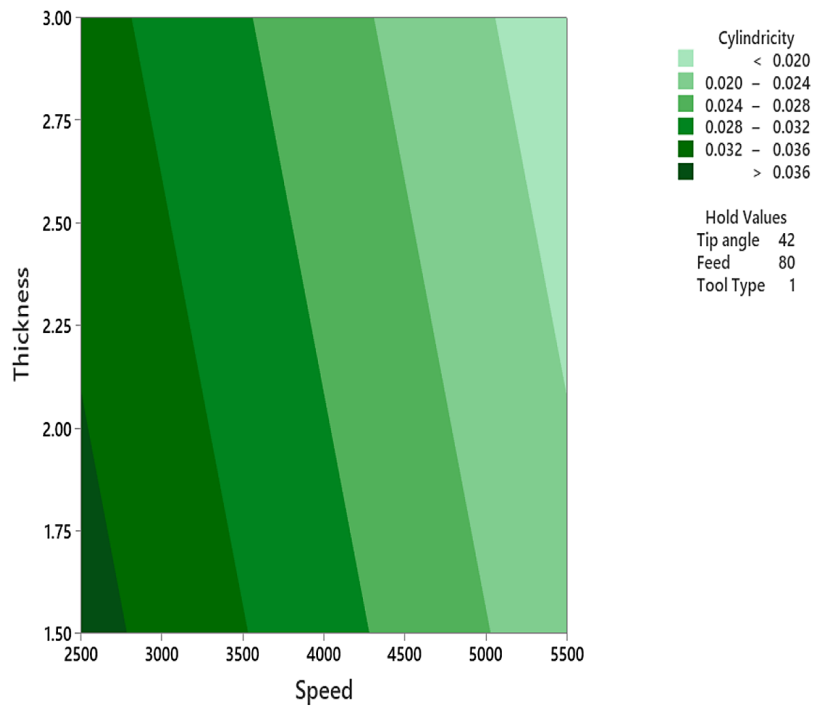


Figure 26. Contour plot of cylindricity errors vs thickness, speed

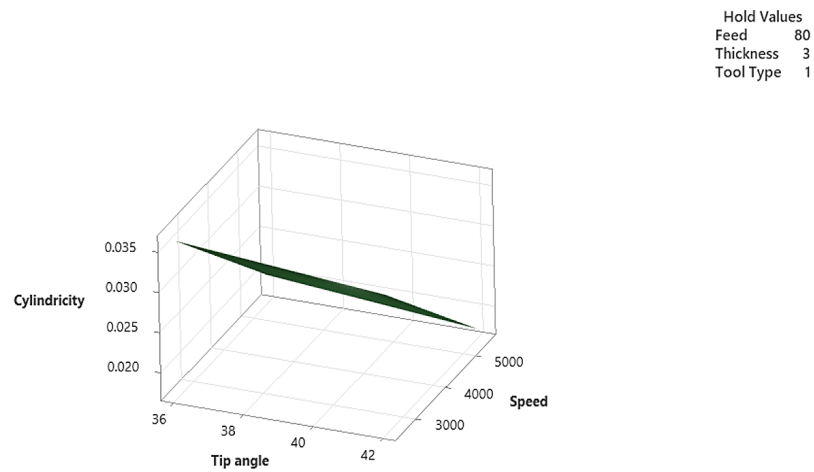


Figure 27. Surface plot of cylindricity errors vs speed, tip angle

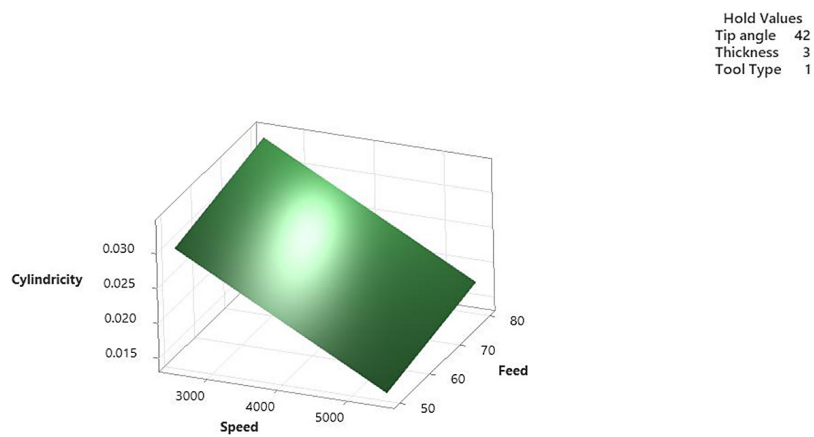


Figure 28. Surface plot of cylindricity errors vs feed, speed

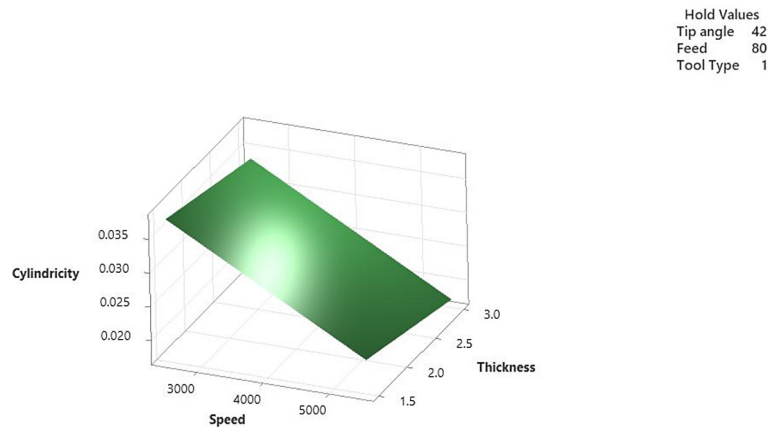


Figure 29. Surface plot of cylindricity errors vs speed, tip angle

Table 13. ANOVA for hole size

Source	Contribution	Adj SS	Adj MS	F-Value	P-Value
Tip angle	8.20%	0.000308	0.000308	9.28	0.041
Speed	10.67%	0.001349	0.001349	14.21	0.034
Feed	11.21%	0.005067	0.005067	14.55	0.031
Thickness	5.07%	0.000107	0.000107	7.53	0.051
Tool type	45.93%	0.094105	0.094105	54.43	0
Error	18.92%	0.053503	0.001115		
Total	100.00%				
R- Sq	87.32%				

surface plot that higher spindle speed and lower feed is favorable as it produces better and close dimension hole size.

It is found that with increase in spindle speed spindle speed continues to help slightly enlarge the hole size, possibly by maintaining smooth tool engagement whereas with increase in thickness causes a small reduction in hole size due to forces. For higher speed and less thickness, the best hole size is observed, which can be confirmed in the surface plot that higher spindle speed and lower thickness is favorable as it produces better hole size (Table 14) (Figures 30–32).

Artificial neural network

ANN with 5 input and 5 output parameters with one hidden layer of 10 neuron

ANNs are computational models inspired by the way biological neural systems process

information. They are especially useful in solving complex problems like pattern recognition and intelligent prediction, which are difficult to automate but are naturally handled by animals. In this study, an ANN model was developed to predict key outputs in the friction drilling process, including thrust force, torque, roundness error error, cylindricity errors error, and hole size. The model was trained using experimental data, and the Levenberg-Marquardt algorithm was selected due to its efficiency in minimizing prediction errors. After testing various configurations, the optimal network architecture was found to have five input neurons, ten neurons in the hidden layer, and five output neurons (Figures 33–39).

The final model structure is illustrated through MATLAB plots, which show how the ANN performed during training, validation, and testing. At 1000 training epochs, the model achieved a minimum MSE of 0.0010756. The

Table 14. Trend of main effect plot for hole size

Output variable	Tip angle	Speed	Feed	Thickness	Tool type
Hole size	Positive	Positive	Positive	Positive	Positive

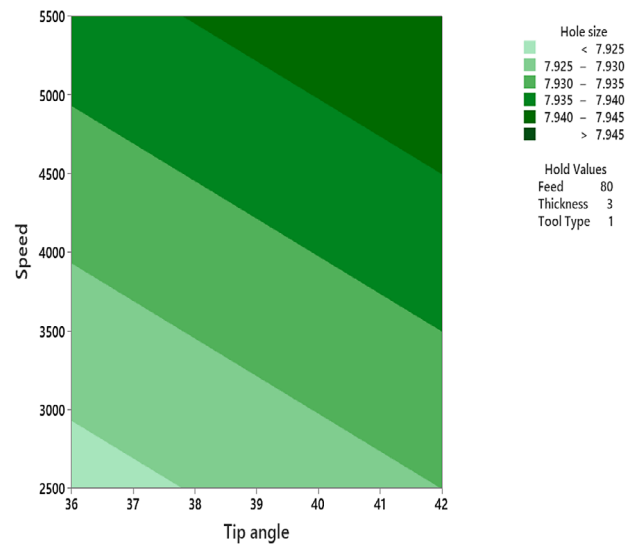


Figure 30. Contour plot of hole size vs speed, tip angle

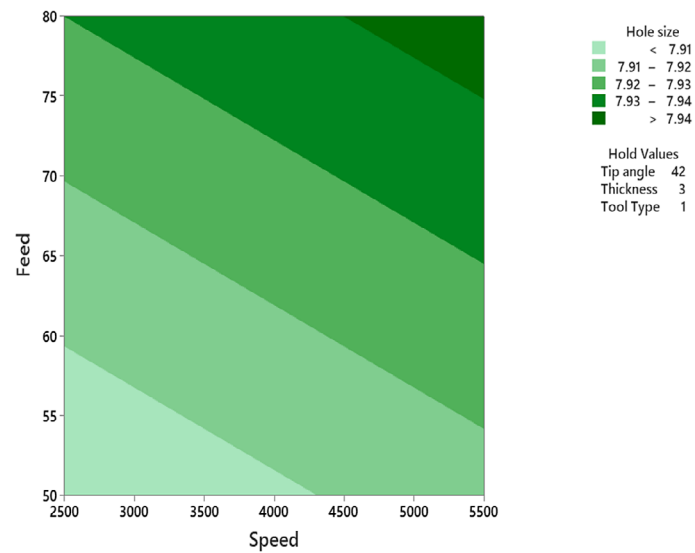


Figure 31. Contour plot of hole size vs feed, speed

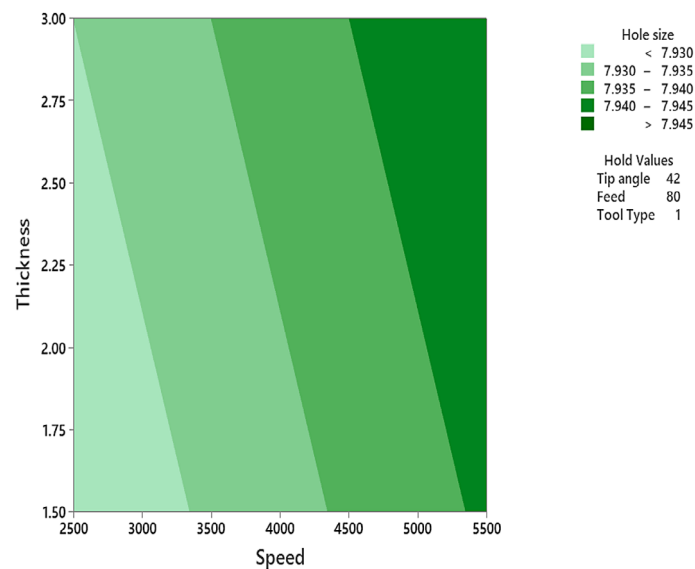


Figure 32. Contour plot of hole size vs thickness, speed

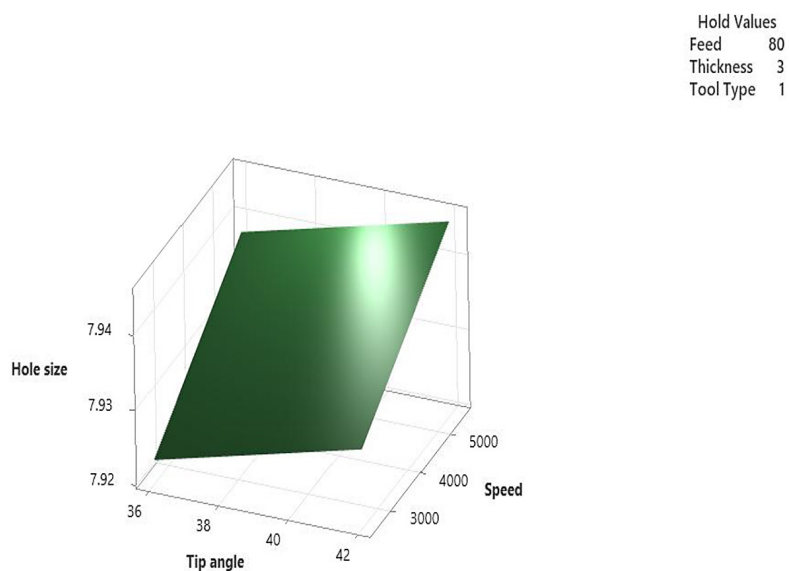


Figure 33. Surface plot of hole size vs speed, tip angle

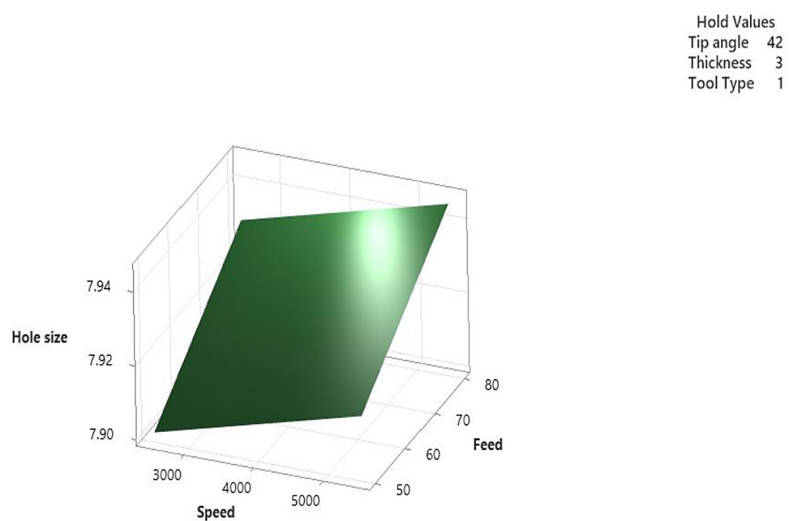


Figure 34. Surface plot of hole size vs feed, speed

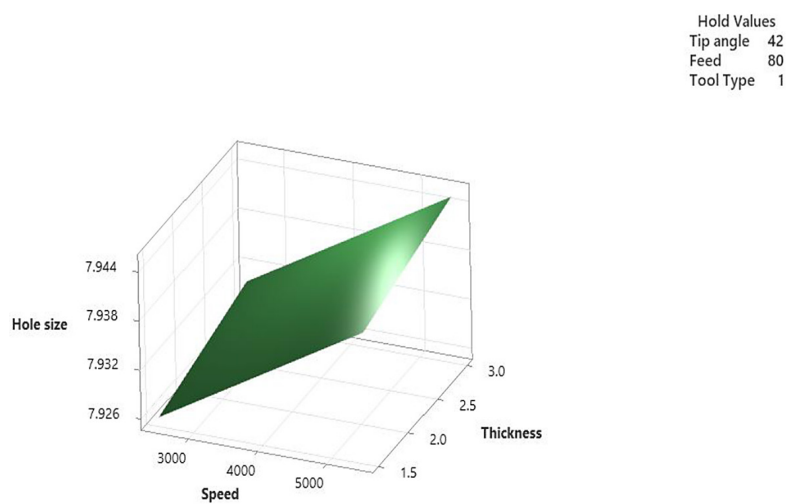


Figure 35. Surface plot of hole size vs speed, tip angle

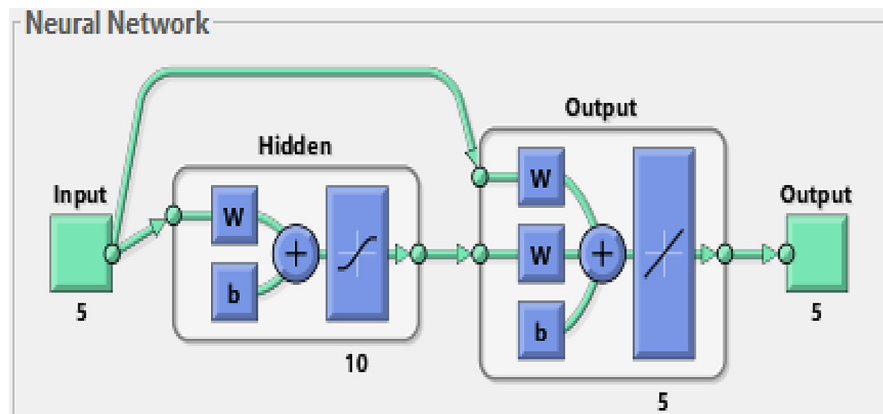


Figure 36. ANN network diagram

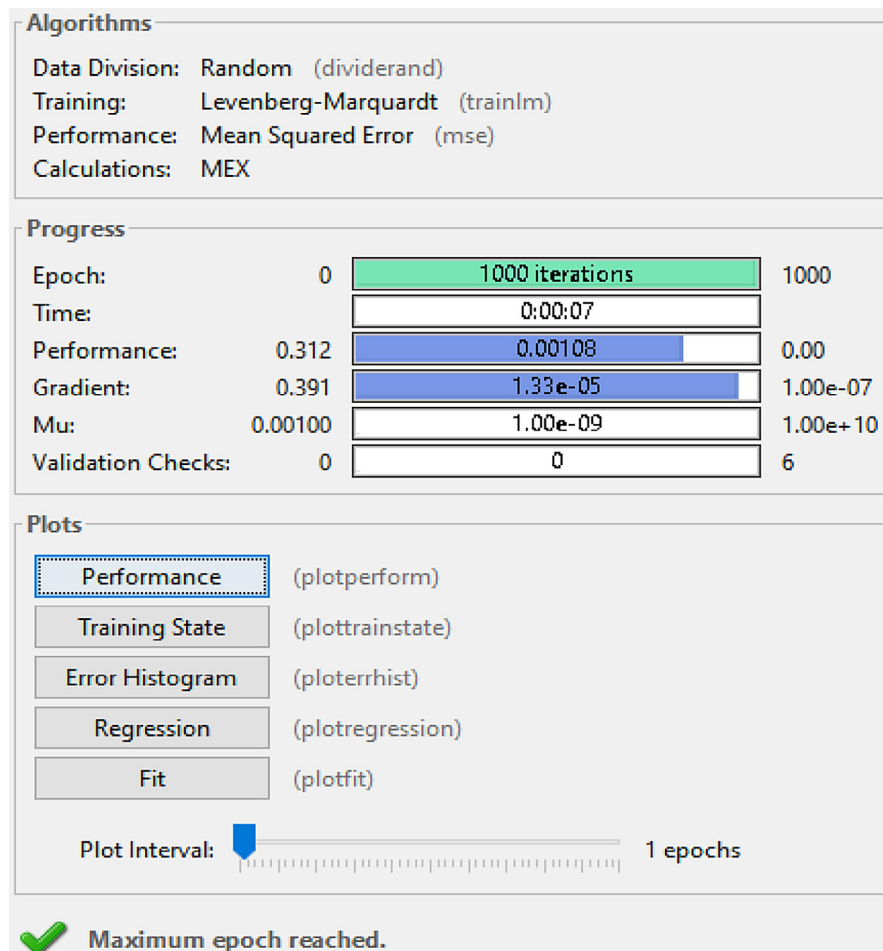


Figure 37. Depiction of the ANN topology

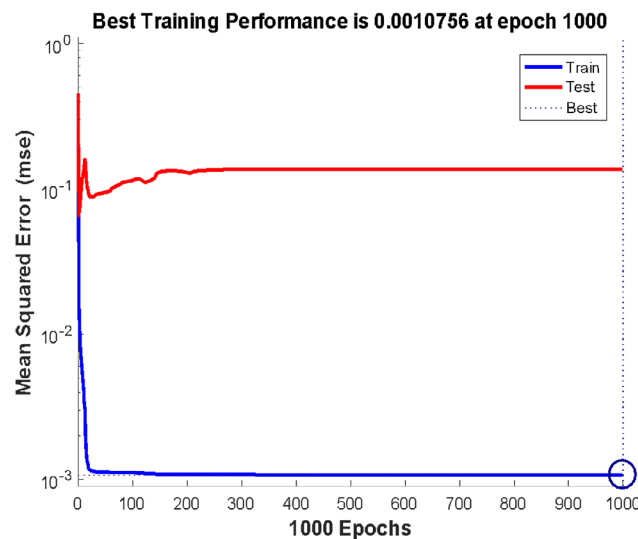


Figure 38. Mean square error



Figure 39. MSE

error histogram revealed that most predictions were tightly clustered around the zero-error line, indicating high accuracy. The regression plots for training, testing, and validation data further confirmed the strong correlation between predicted and actual values, with an average R^2 value of 99.55%, which reflects excellent prediction capability. Additional validation runs were also conducted, and all predictions showed less than 5% error, confirming the model's reliability (Figure 40–42).

The ANN was implemented using MATLAB, where a feed-forward neural network structure was used to model and optimize the drilling parameters. Compared to traditional

multiple regression methods, ANN offers better adaptability, faster learning, and higher prediction accuracy. The ANN not only predicted hole size and shape errors but also helped identify the best drilling settings to reduce defects. The Levenberg-Marquardt algorithm was used to update network weights during training, based on an iterative process that minimizes the cumulative error. This process involves adjusting weights, calculating new errors, and continuing until the error is reduced below a set threshold. The MSE was the main performance metric used to evaluate the model, and several runs were performed with randomly divided data to ensure accuracy and consistency (Table 15 and 16).

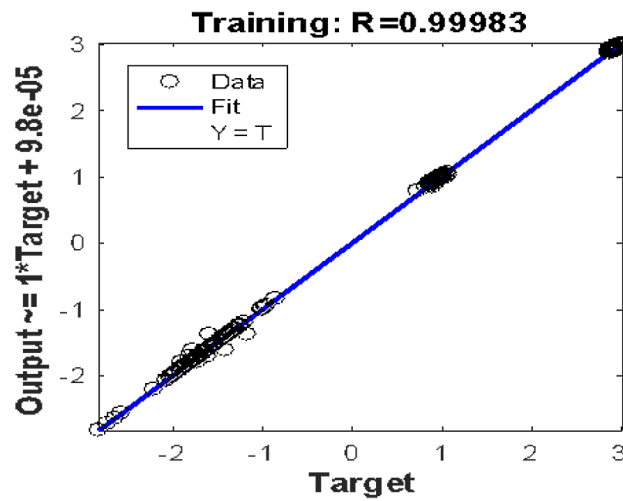


Figure 40. Histogram for ANN training data

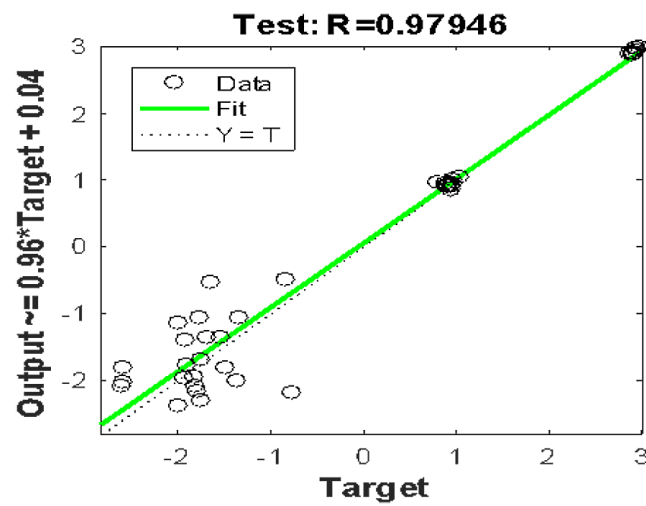


Figure 41. Histogram for ANN test data

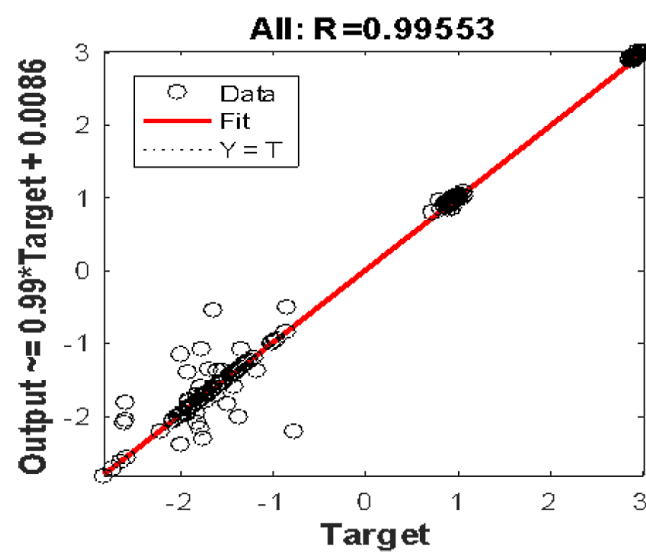


Figure 42. Histogram for ANN model all

Table 15. Target vs predicted value obtained from ANN

Target value					Predicted value				
Thrust force	Torque	Roundness error	Cylindricity error	Hole size	Thrust force	Torque	Roundness error	Cylindricity error	Hole size
N	Nm	mm	mm	mm	N	Nm	mm	mm	mm
798.27	7.93	0.001	0.014	8	771.49	7.03	0.001	0.014	7.99
810.2	6.436	0.017	0.012	7.92	793.65	9.24	0.0182	0.016	7.89
894.1	10.07	0.0459	0.016	7.92	884.66	10.49	0.045	0.016	7.9
839.2	8.89	0.0122	0.01	7.99	791.26	7.82	0.0129	0.011	8.02
901.23	9.934	0.0568	0.113	7.92	982.36	10.17	0.056	0.113	7.92
827	8.89	0.022	0.063	8	765.6	8.77	0.021	0.063	7.98
892.22	10.14	0.035	0.023	8	829.44	10.38	0.035	0.023	7.98
895.3	9.832	0.012	0.011	8	893.65	10.28	0.012	0.011	7.99
829.9	8.9	0.024	0.025	8	851.31	8.76	0.024	0.026	8
901.8	12.05	0.051	0.045	8	884.76	10.57	0.051	0.044	7.99
824.5	10.05	0.023	0.012	7.92	827.36	10.07	0.024	0.015	7.92
960.3	9.06	0.002	0.013	7.92	938.15	9.73	0.002	0.013	7.9
801.1	8.456	0.008	0.022	8	835.61	8.56	0.008	0.022	8.04
835.4	9.23	0.018	0.018	7.9	858.09	8.83	0.018	0.018	7.94
750.33	7.438	0.006	0.016	7.92	802.91	7.62	0.006	0.016	7.93
798.2	10.129	0.019	0.022	8	838.71	10.13	0.019	0.022	8
800.1	10.1	0.043	0.012	7.92	882.02	10.62	0.043	0.0128	7.86
894	7.889	0.01	0.015	7.92	879.54	8.3	0.01	0.015	7.92
830.21	8.455	0.002	0.033	7.92	793.55	9.08	0.0021	0.035	7.9
882.76	9.05	0.02	0.023	7.92	895.93	9.34	0.02	0.023	7.89
802.41	6.87	0.009	0.025	7.92	777.33	6.89	0.009	0.025	7.93
892.44	7.79	0.016	0.015	7.84	860.03	8.62	0.016	0.017	7.9
801.14	7.99	0.036	0.04	8	815.13	8.77	0.036	0.04	7.99
749.32	5.45	0.012	0.039	8	751.21	6.16	0.012	0.039	8
856.57	9.76	0.023	0.029	8	894.28	9.95	0.024	0.029	7.97
950.34	11.02	0.0436	0.023	7.92	962.05	10.74	0.045	0.0244	7.96
823.84	7.6	0.008	0.108	8.1	820.26	7.27	0.008	0.108	8.06

Table 16. Mean absolute percentage error

Parameter	Thrust force	Torque	Roundness error	Cylindricity error	Hole size
MAPE	3.50486	6.47267	1.39325	3.95197	0.26097

The experimental setup used to generate training data followed a RSM approach, using five input variables, each tested at three levels with one repeat – resulting in 54 total experimental combinations. When evaluating the model’s prediction performance, the average error percentages were found to be remarkably low: 0.350486% for thrust force, 0.647267% for torque, 0.139325% for roundness error error, 0.395197% for cylindricity error, and just 0.026097% for hole size. The overall correlation coefficient (R-value) of

0.9953 indicates a very strong match between predicted and experimental results. This confirms the ANN model’s effectiveness and suitability for real-time application in optimizing the friction drilling process (Table 16).

CONCLUSIONS

In the friction drilling of AL 6063, tool geometry plays a significant role, slotted center

drills generate more thrust force than plain ones, as they perform both cutting and forming in a single pass, while plain drills only form the material.

The ANOVA results reveal that spindle speed consistently has the most significant impact across all responses, with contributions of 27.16% to thrust force, 49.81% to torque, 48.19% to roundness error, and also improving cylindricity error and hole size when increased.

Increase in spindle speed leads to a noticeable reduction in thrust force by 20–30%, torque by 30–45%, roundness error by 35–40%, and cylindricity error, as confirmed in surface plots.

Thickness significantly affects thrust force 18.78% and torque 4.71%, with larger thickness resulting in increased cutting loads and geometric errors. Feed contributing 3.98% to thrust force, 5.67% to torque, 4.44% to roundness error, and 4.48% to hole size, where increasing feed slightly increases load and geometric error.

Tip angle influences roundness error shows a small effect on other responses, while tool type is dominant for cylindricity error 49.44% and hole size 45.93%, confirming plain center drill has perform well over slotted center drill. Key parameters like tool type, speed, feed, and thickness directly influence hole quality, including cylindricity, circularity, and size. ANOVA results show that cylindricity error is governed by speed and feed, circularity by speed and thickness, and hole size by tool geometry and other process factors.

Spindle speed and thickness are the most contributing parameters in thrust force, higher spindle speed and lower thickness is favorable as it produces lower thrust force as a result less load is applied on tool and machine.

Increase in spindle speed decreases overall Torque as this allows easy penetration into material of varying thickness and improves roundness error of drilled hole getting results closer to expected

Type of tool is significant in reducing circularity error and hole size SCD tool outperforms in getting better results, by decreasing overall cylindricity error. The ANN prediction model demonstrated strong reliability, with prediction errors ranging from 0.23% to 6.47%, a best training score of 0.0010756, and an average R^2 value of 99.53%, confirming its effectiveness in predicting friction drilling performance across varying conditions.

REFERENCES

1. Miller, S. F., Tao, J., Shih, A. J. Friction drilling of cast metals. *International Journal of Machine Tools and Manufacture*, 2006; 46(12–13), 1526–1535, <https://doi.org/10.1016/j.ijmachtools.2005.09.003>
2. Lee, S. M., Chow, H. M., Huang, F. Y., Yan, B. H. Friction drilling of austenitic stainless steel by uncoated and PVD AlCrN- and TiAlN-coated tungsten carbide tools, *International Journal of Machine Tools & Manufacture* 2009; 49, 81–88. <https://doi.org/10.1016/j.ijmachtools.2008.07.012>
3. El-Bahloul, S. A., El-Shourbagy, H. E. and El-Midany, T. T. Optimization of thermal friction drilling process based on Taguchi method and fuzzy logic technique, *International Journal of Science and Engineering Applications*, 2015; 4(2), <http://dx.doi.org/10.7753/IJSEA0402.1006>
4. Schulze, V., Zanger, F., Michna, J., Lang, F. 3D-FE-Modelling of the Drilling Process – Prediction of Phase Transformations at the Surface Layer, 14th CIRP Conference on Modeling of Machining Operations, *Procedia CIRP* 8. 2013; 33–38, <https://doi.org/10.1016/j.procir.2013.06.061>
5. Pantawane, P. D., Ahuja, B. B. Experimental investigations and multi-objective optimization of friction drilling process on AISI 1015, *International Journal of Applied Engineering Research*, Dindigul, 2011; 2(2).
6. Dehghan, S., Soury, E. A comparative study on machining and tool performance in friction drilling of difficult-to-machine materials AISI 304, Ti-6Al-4V, Inconel 718. *Journal of Manufacturing Processes*, 2021; 61, 128–152, <http://dx.doi.org/10.1016/j.jmapro.2020.10.078>
7. Dehghan, S., Shah, M. I., Soury, E. I. A thermo-mechanical finite element simulation model to analyze bushing formation and drilling tool for friction drilling of difficult-to-machine materials, *Journal of Manufacturing Processes* 2020; 57, 1004–1018, <http://dx.doi.org/10.1016/j.jmapro.2020.07.022>
8. Rao, K. H., Gopichand, A., Kumar Pavan N. and Jitendra, K. Optimization of machining parameters in friction drilling process, *International Journal of Mechanical Engineering and Technology (IJMET)*, April 2017; 8(4), 242–254.
9. Alphonse, M. Raja, V. B., Palanikumar, K., Sanjay, D. S. K., Subbaiah, B. V., Chandra, L. V. Highlights of non-traditional friction drilling process: A review. *Materials Today: Proceedings*, 2021. <http://dx.doi.org/10.1016/j.matpr.2021.01.336>
10. Miller, S. F., Blau, P. J. and Shih, A. J. Tool wear in friction drilling. *International Journal of Machine Tools and Manufacture* 2007; 47(10), 1636–1645, <https://doi.org/10.1016/j.ijmachtools.2006.10.009>
11. Yerriswamy, M., Sreenivasulu, B., Ramachandra, R. Modelling and analysis of friction drilling process

- using RSM, *International Journal of Engineering Science and Computing*. 2016 IJESC.
12. Miller, S. F., Blau, P. J. and Shih, A. J. Microstructural alterations associated with friction drilling of steel, aluminum, and titanium, *JMEPEG* 2005; 14, 647–653, <http://dx.doi.org/10.1361/105994905X64558>
13. Ozek, C., Demir, Z. Investigate the friction drilling of aluminium alloys according to the thermal conductivity, *TEM Journal* 2013; 2(1).
14. Biermann, D., Liu, Y. Innovative flow drilling on magnesium wrought alloy AZ31, *Procedia CIRP* 2014; 18, 209–214. <https://doi.org/10.1016/j.procir.2014.06.133>
15. Potdar, A., Sapkal, S. Optimization of friction drilling process by response surface methodology. In *Advanced Engineering Optimization through Intelligent Techniques* 2020; 351–359. Springer, Singapore, http://dx.doi.org/10.1007/978-981-13-8196-6_31
16. Mustafa, Z., Idrus, N. H., Hadzley, A. B. M., Sivakumar, D., Norazlina, M. Y., Fadzullah, S. H. S. M., Thongkaew, K. Optimization of drilling process parameters on delamination factor of Jute reinforced unsaturated polyester composite using Box-Behnken design of experiment. *Journal of Mechanical Engineering and Sciences*, 2020; 14(1), 6295–6303. <https://doi.org/10.15282/jmes.14.1.2020.08.0493>
17. Ku, W.-L., Hung, C.-L., Lee, S.-M., Chow, H.-M. Optimization in thermal friction drilling for SUS 304 stainless steel *International Journal Advanced Manufacturing Technology* 2011; 53, 935–944, <http://dx.doi.org/10.1007/s00170-010-2899-5>
18. Gopal, K. P. V., Kishore, K. and Satyanarayana, V. V. Some investigations in friction drilling AA6351 using high speed steel tools. *Engineering and Applied Sciences* 2010; 5(3), 11–15.
19. Chow, H.-M., Lee, S.-M., Yang, L.-D. Machining characteristic study of friction drilling on AISI 304 stainless steel. *Journal of materials processing technology* 2008; 207. <https://doi.org/10.1016/j.jmatprotec.2007.12.064>
20. Agarwal, Gunjan, and Khare, M. K. Multi objective optimization of cutting parameters in machining—a sustainable approach. *Materials Today: Proceedings* 2020, <https://doi.org/10.1016/j.matpr.2020.09.272>
21. Kaviarasan, V., Venkatesan, R. and Natarajan, E. Prediction of surface quality and optimization of process parameters in drilling of Delrin using neural network. *Progress in Rubber, Plastics and Recycling Technology* 2019; 35(3), 149–169. <https://doi.org/10.1177/1477760619855078>
22. Dol, optimalna, jekla z. Uporabo, and undented nevronske. Optimum bushing length in thermal drilling of galvanized steel using artificial neural network coupled with genetic algorithm. *Material in Technology* 2017; 51(5), 813–822, <http://dx.doi.org/10.17222/mit.2016.290>
23. Mutalib, M. Z. A., Ismail, M. I. S., As'array, A. and Abdul N. A. Multi-objective optimization in friction drilling of aisi1045 steel using grey relational analysis.
24. Selvaraj, R. M., and Hynes N. R. J. Finite element approach in thermal modelling of friction stud welding. In *AIP Conference Proceedings*, 2142(1), 110006. AIP Publishing LLC, 2019, <https://doi.org/10.1063/1.5122466>
25. Sharma, V. K., Kumar, V., Joshi, R. S. and Sharma, D. Experimental analysis and characterization of SiC and RE oxides reinforced Al-6063 alloy based hybrid composites. *The International Journal of Advanced Manufacturing Technology* 2020; 108(4), 1173–1187.
26. Skovron, J. D., Prasad, R. R., Ulutan, D., Mears, L., Detwiler, D., Paolini, D., Baeumler, B., and Claus, L. Effect of thermal assistance on the joint quality of Al6063-T5A during flow drill screw driving. *Journal of Manufacturing Science and Engineering* 2015, 137(5).
27. Kamble, Y., Rajiv, B. (2021). Experimental investigation and dimensional analysis of friction drilled hole on 6082 aluminium pipe using hardened M2 High Speed Steel centre drill ,*Materials today proceedings*, 2021; 42, Part 2, 1239–1243. <http://dx.doi.org/10.1016/j.matpr.2020.12.874>
28. Kamble, Y. G., Pantawane, P. D., Rajiv, B., Ahuja, B. B. (2020). Design and Development of Combination Tool for Drilling and Tapping Operation on PVC. In: Shunmugam, M., Kanthababu, M. (eds) *Advances in Simulation, Product Design and Development. Lecture Notes on Multidisciplinary Industrial Engineering*. Springer, Singapore. https://doi.org/10.1007/978-981-32-9487-5_44
29. Rathod, V. P., Wankhade, S. H. A review on impact of micro-tools on micro-milling outcomes for aluminium alloy. *Advances in Science and Technology Research Journal*, 2025; 19(3), 322–340. <https://doi.org/10.12913/22998624/200007>
30. Rathod, V. P., Wankhade, S. H. Comprehensive review of tool treatments and innovations in micro-milling precision and performance. *Advances in Science and Technology Research Journal*, 2025; 19(4), 241–257. <https://doi.org/10.12913/22998624/200545>
31. Rathod, V. P., Wankhade, S. H., Kamble, Y. G. Evaluating the efficiency of micro end mill tools and performance metrics in micro milling. *Journal of Mines, Metals and Fuels*, 2025; 73(7), 2253–2265. <https://doi.org/10.18311/jmmf/2025/49414>